PHYSICAL REVIEW B VOLUME 27, NUMBER 7 1 APRIL 1983

4f- and core-level photoemission satellites in cerium compounds

Atsushi Fujimori
National Institute for Research in Inorganic Materials, Sakura-mura, Niihari-gun, Ibaraki 305, Japan
(Received 4 October 1982)

The two 4f-derived photoemission features recently observed for Ce pnictides are identified with hybridized 4f-hole and ligand-hole final states. Simple expressions obtained for a CeX_6 cluster explain the change in the relative intensity of the two 4f features without energy shifts. Analogous expressions are presented for the satellite structures of the 3d core x-ray-photoemission spectra of rare-earth compounds, assuming a "poorly screened" core-hole state and a core-hole state screened by 4f-electron—ligand-hole excitations with hybridization between these core-hole states. It is shown that in some lanthanum compounds the high—binding-energy line is due to a "well-screened" core hole arising from the ligand→4f shakeup process while for other rare-earth compounds the "well-screened" peak lies at lower binding energies. It is also suggested that the extra intensities in the bremsstrahlung-isochromat spectra of Ce and its alloys are due to final-state effects arising from hybridized $4f^2$ and $4f^1$ configurations.

I. INTRODUCTION

The electronic structure of cerium and its compounds has attracted much interest both experimentally and theoretically, because they exhibit anomalous physical properties which have been attributed to 4f electrons. The Ce 4f state is delocalized in some compounds and is localized in others. When the 4f level is located close to the Fermi energy E_F, Ce compounds exhibit mixed valency.[1] Photoelectron spectroscopy is a powerful tool in studying the 4f-electron state, but for localized or narrow-band systems such as 4f electrons in cerium compounds one cannot ignore correlation effects induced by a photohole. In such a case, photoelectrons give the total energy of the excited final state rather than one-electron energy levels in the initial ground state.[2] Satellite structures of the 3d valence bands of Ni,[3] Cu,[4] Zn,[5] Ni compounds,[6] etc., have been attributed to final-state effects.

Very recently two 4f-derived photoemission features have been observed for Ce pnictides.[7] Similar satellite structures have also been reported for a 5f system UAsSe.[8] By varying photon energy to enhance the Ce 4f component (just above the 4f emission threshold or the 4d→4f resonance threshold), two 4f-related features have been observed at binding energies of 0.6 and about 3 eV for CeP, CeAs, and CeBi, and have been identified, respectively, with a partially delocalized hole resulting from the 4f—pnictide p hybridization and with a localized 4f hole screened by 5d electrons. The intensity ratio of the 0.6-eV peak to the 3-eV peak decreases on going from CeP to CeAs to CeBi while the total 4f emission strength remains constant. These authors claim that reexamination of the 4f levels in Ce compounds are necessary.[7] The satellite structures of UAsSe have also been attributed to delocalized and localized 5f holes in the final state.[8]

In the present paper, a simplified theoretical model is presented for the satellite structures of the 4f-related photoemission using Ce-ligand clusters. The problem is reduced to interactions between two final states corresponding to a localized 4f hole and correlated 4f-electron—ligand-hole pair. This model explains the energies and relative intensity of the two 4f features in terms of the hybridization of the two final states. Somewhat different identification than the original one[7] is presented as will be shown in Sec. II.

An analogous treatment with two final states will be shown to account for the intensities and energies of the so-called shakeup (shakedown) satellites in the 3d core-level x-ray-photoemission spectra (XPS) of Ce compounds and other rare-earth compounds (Sec. III). The two final states correspond to a poorly screened 3d hole and a 3d hole screened by correlated 4f-electron—ligand-hole excitations. Relation between the 4f and 3d spectra of the Ce pnictides[9] is discussed based on this model. The 3d spectra of rare-earth oxides,[10] rare-earth hydrides,[11] etc., are also discussed.

Finally in Sec. IV it is proposed that the extra intensities in the bremsstrahlung-isochromat spectra

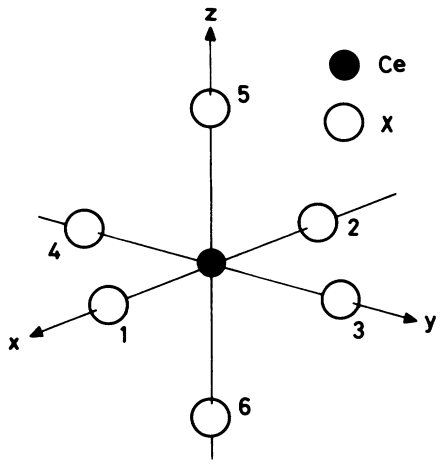

FIG. 1. Structure of the LX_6 cluster representing local environment of the rare-earth ion in rare-earth monopnictides.

(BIS) of Ce and its alloys[12] can be attributed to hybridization between the localized $4f^2$ configuration and the delocalized state with the incident electron in empty valence states. The extra intensity for γ-Ce, $CeSn_3$, and $CePd_3$ just above E_F have been previously interpreted in terms of empty $4f^1$ levels.[12] It is shown that the hybridization between the two final states gives qualitatively an explanation in a more consistent way.

II. SATELLITES IN 4f-DERIVED PHOTOEMISSION

The Ce monopnictides CeX crystallize in the NaCl structure. A CeX_6 cluster shown in Fig. 1 is considered. The initial state of the Ce ion is assumed to be $4f^1$ with localized magnetic moment, and ligand p orbitals to be filled (actually the ligand orbitals are Ce $5d$–X p bonding orbitals rather than pure p orbitals). The initial ground state of the CeX_6 cluster is written as

$$\Psi_I = |4f\rangle \ . \tag{1}$$

As we are concerned with the $4f$-derived emission, the final state can be represented as a linear combination of the $4f$-hole state and ligand-hole states as

$$\Psi_F = c_{F0}|4f^0\rangle + \sum_l c_{Fl}\phi_l \ , \tag{2}$$

$$\phi_l = (1/\sqrt{2})\sum_\sigma \phi_{l\sigma} = \sum_{i,j,\sigma} \Gamma^l_{ij} | L^{-1}_{i\sigma} 4f_{j\sigma}\rangle \ , \tag{3}$$

where $L^{-1}_{i\sigma}$ represents a hole in the ligand orbital $L_{i\sigma}$ and $4f_{j\sigma}$ is a $4f$ electron in the jth crystal-field level with spin σ. Γ_{ij}'s restrict the second term in (2) to have the full symmetry of the cluster. Under the condition that the $4f$ emission dominates p-derived emission,[7] the emission intensity becomes

$$I \simeq |c_{F0}\langle 4f|e\vec{r}|\epsilon l\rangle|^2 \propto |c_{F0}|^2 \ . \tag{4}$$

c_{F0} and the final-state energy are obtained by solving

$$\sum_{l'} H_{ll'} c_{Fl'} = E c_{Fl} \ . \tag{5}$$

Nonzero off-diagonal elements $H_{ll'}$ have the form of $V = \langle 4f^0 | H | \phi_l \rangle$. If only the largest V is retained in (5), we only have to deal with a 2×2 Hamiltonian,

$$H = \begin{bmatrix} 0 & V \\ V & \epsilon_{4f} - \epsilon_L \end{bmatrix} , \tag{6}$$

where ϵ_{4f} and ϵ_L are the orbital energies of the $4f^1$ and appropriate ligand levels.

If there are two non-negligible V's, one can use instead of ϕ_l and ϕ_m,

$$\phi_1 = (V_l\phi_l + V_m\phi_m)/(V_l^2+V_m^2)^{1/2} \ ,$$

$$\phi_2 = (V_m\phi_l - V_l\phi_m)/(V_l^2+V_m)^{1/2} \ .$$

By using them,

$$\langle 4f^0 | H | \phi_1\rangle = (V_l^2+V_m^2)^{1/2} \ ,$$

$$\langle \phi_1 | H | \phi_1\rangle = \epsilon_{4f} - (\epsilon_L^l V_l^2 + \epsilon_L^m V_m^2)/(V_l^2+V_m^2)^{1/2} \ ,$$

where ϵ_L^l and ϵ_L^m are the energies of the ligand orbitals in ϕ_l and ϕ_m. $\langle \phi_1 | H | \phi_2\rangle$ can be neglected if one of the two V's is predominant or $\epsilon_L^l \simeq \epsilon_L^m$, which is satisfied in most cases. Thus the problem is again reduced to the 2×2 matrix with $V = (V_l^2+V_m^2)^{1/2}$ and

$$\epsilon_L = (V_l^2\epsilon_L^l + V_m^2\epsilon_L^m)/(V_l^2+V_m^2)^{1/2} \ .$$

Extension to cases with more than three ϕ's is easy.

By solving (5) with (6), two final states with energies $E_\pm$ are obtained. Two $4f$ photoemission lines appear at binding energies

$$E_B = E_\pm - \epsilon_{4f}$$
$$= \{-\epsilon_{4f} - \epsilon_L \pm [(\epsilon_{4f}-\epsilon_L)^2 + 4V^2]^{1/2}\}/2 \ , \tag{7}$$

with intensity ratio

$$I_-/I_+ \simeq |c_{-0}/c_{+0}|^2$$
$$= [(x^2+4)^{1/2}+x]/[(x^2+4)^{1/2}-x] \ , \tag{8}$$

$$x = (\epsilon_{4f}-\epsilon_L)/|V| \ . \tag{9}$$

Equation (7) indicates that for $|\epsilon_{4f}-\epsilon_L| \ll 2|V|$

the separation between the two lines is $\sim 2|V|$ independent of $\epsilon_{4f}-\epsilon_L$, while the relative intensity varies sensitively with $\epsilon_{4f}-\epsilon_L$. This is illustrated in Fig. 2, where $(\epsilon_{4f}-\epsilon_L)/|V|$ for CeP, CaAs, and CeBi obtained from the intensity ratio[7] is indicated. ϵ_L is lowered for the series CeBi→CeAs→CeBi as is evident from the position of the p-derived valence-band emission,[7] while ϵ_{4f} rises. Hence the binding energies of the two $4f$-derived features separated by $\sim 2|V|$ do not shift and the relative intensity changes drastically. The "bare" $4f$ and ligand orbital energies, ϵ_{4f} and ϵ_L, have been obtained using Eqs. (7)—(9) and are listed in Table I. ϵ_L's thus obtained correspond to the valence-band peak or slightly above it. The value $|V| \sim 1$ eV is reasonable and is fairly constant over the pnictides (Table I). Thus our assignment differs from that in Ref. 7 in that we have identified the stronger features with the localized $4f$-hole state and the weaker ones with delocalized hole states while in Ref. 7 they have attributed the high—binding-energy features and the low—binding-energy features, respectively, to $5d$-screened localized $4f$-hole and delocalized hole states.

$4f$ and ligand orbitals involved in the final states are of two types: t_{1u}-like orbitals and t_{2u}-like ones. t_{1u}-like $4f$ and ligand orbitals form σ bonds and t_{2u}-like ones form π bonds. Thus the electron-hole pair that couples most effectively with the $4f$ emission is a linear combination of the following two states:

$$\phi_{l\sigma}=(1/\sqrt{3})\{(1/\sqrt{2})(x_1+x_2)[x^3-(\tfrac{3}{5})xr^2]+(1/\sqrt{2})(y_3+y_4)[y^3-(\tfrac{3}{5})yr^2]$$
$$+(1/\sqrt{2})(z_5+z_6)[z^3-(\tfrac{3}{5})zr^2]\}\ ,$$

$$\phi_{m\sigma}=(1/\sqrt{3})\{(\tfrac{1}{2})(z_1+z_2-z_3-z_4)[(x^2-y^2)z]+(\tfrac{1}{2})(x_3+x_4-x_5-x_6)[(y^2-z^2)x]$$
$$+(\tfrac{1}{2})(y_5+y_6-y_1-y_2)[(z^2-x^2)y]\}\ ,$$

for t_{1u} and t_{2u}, respectively, where x_1 denotes the p_x orbital on the X atom 1 of Fig. 1, etc. ϵ_L may be estimated from energy levels of the band structure as $\epsilon_L^l(t_{1u})\simeq[\epsilon(X_4')+\epsilon(\Gamma_{15})]/2$ because $L(t_{1u}^z)\simeq[\psi(X_4'(001))+\psi(\Gamma_{15}^z)]/\sqrt{2}$, and $\epsilon_L^m(t_{2u})\simeq\psi(\Sigma_3)$ because $L(t_{2u}^z)\simeq\psi(\Sigma_3(\frac{1}{2}\frac{1}{2}0))$. Band structures have been calculated for Gd pnictides GdX (X=N, P, As, and Sb).[13] In these results, the above ϵ_L's are found near or slightly above the density-of-states (DOS) peak of the p-derived valence bands in agreement with ϵ_L in Table I deduced from experiment.

Ligand orbitals L appearing in $|L^{-1}4f\rangle$ do not have the Ce $5d$ component because within the cluster approximation molecular orbitals with odd symmetry are allowed in (3). In the final state of photoemission, terms of the form $\langle 4f^0|H|L^{-1}5d\rangle$ where L has even symmetry become nonzero due to $4f$-$5d$ on-site interactions. The $\langle 4f^0|H|L^{-1}5d\rangle$ terms serve to screen the $4f$ hole by $5d$ electrons and may also cause the $L\rightarrow 5d$ shakeup excitations. Therefore, $|4f^0\rangle$ in (2) implicitly includes the $5d$ screening terms $|L^{-1}5d\rangle$. However, the $5d$ screening of the $4f$ hole is not so important as in metallic Ce and alloys due to a low $5d$ DOS in the region near E_F.

Here the initial state (1) has been treated as a localized $4f^1$ configuration with energy ϵ_{4f}. ϵ_{4f} in Table I varies by as much as ~ 1 eV, much larger

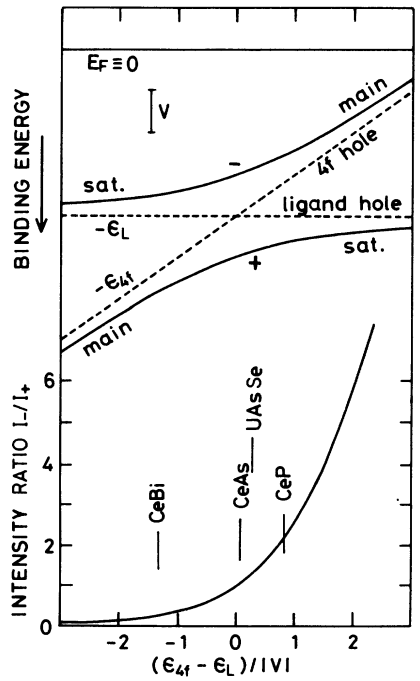

FIG. 2. Binding energies and intensity ratio of two $4f$-derived photoemission features of Ce pnictides as a function of $(\epsilon_{4f}-\epsilon_L)/|V|$. The value for $(\epsilon_{4f}-\epsilon_L)/|V|$ is indicated for CeP, CeAs, CeBi and a $5f$ compound UAsSe.

TABLE I. The energies of the $4f$ level ϵ_{4f} and the ligand level ϵ_L and the effective matrix element V for Ce pnictides obtained from observed intensity ratios and binding energies of $4f$-related emission features. All energies in electron volts.

	Binding energies[a] E_B	Intensity ratio[a] I_-/I_+	ϵ_{4f}	ϵ_L	V
CeP	0.6,3.1	2.3	−1.4	−2.3	1.2
CeAs	0.6,2.95	1.1	−1.8	−1.8	1.2
CeBi	0.6,2.95	0.3	−2.4	−1.1	1.0

[a]Reference 7.

than the chemical shifts of the core levels.[9] The variation of ϵ_L and ϵ_{4f} in the opposite direction is the cause of the unshifted energies of the $4f$-derived features. This could be explained qualitatively by the energies of the $4f^1$ levels in the initial ground state as follows: The Ce $4f$ level is very sensitive to the $4f$ occupation number and accommodates one f electron. That is, the $4f$ level shifts so that the $4f^1$ level is occupied and that the $4f^2$ level is empty, which is schematically shown in Fig. 3. Hybridization between the ligand and $4f^1$ levels in the ground state leads to bonding and antibonding levels, both of which should be below E_F in order to make the f-electron number ~ 1. In most Ce compounds including CeP, ϵ_L is lower than ϵ_{4f} as in Fig. 3(a). If the ligand level ϵ_L is higher than ϵ_{4f} as in CeBi [Fig. 3(b)], the $4f^1$ level should be lowered so as to locate the antibonding level below E_F. Hence ϵ_{4f} is low when ϵ_L is high and vice versa, resulting in the unshifted $4f$ features. This initial state may be represented by a Slater determinant $\Psi_I = |L\downarrow b\uparrow a\uparrow|$, where $b\uparrow$ and $a\uparrow$ are the bonding and antibonding combinations of $L\uparrow$ and $4f\uparrow$ with up spin, which is equivalent to $|L\downarrow L\uparrow 4f\uparrow|$, that is, the localized $4f$ configuration (1).

Owing to the localized nature of $4f$ holes, the present cluster model could be in principle extended to metallic systems such as metallic Ce or its alloys. In the case of Ce, twelve nearest-neighbor metal atoms should be involved for the $4f$-excited atom, and the Xp orbitals of CeX are replaced by Ce $5d$ orbitals on the neighboring atoms. Occupied $5d$ levels play the role of ligand orbitals. Simple decomposition into two final states as has been done for the pnictides is not a good approximation, though qualitative argument using the simplified model may be helpful. As unoccupied $5d$ levels are just above E_F, screening effects on the main $4f$ feature would be strong. In analogy with the CeX_6 cluster, hybridization between the localized $5d$-screened $4f$ hole and extended $5d$ hole could give rise to two (or more) $4f$-derived features. Photoemission from $Ce_{0.9}Th_{0.1}$ (Ref. 14) has shown a $4f$ emission just below E_F in addition to the one at the binding energy of about 2 eV, which could be ascribed to the above-mentioned effect. The bare $4f$ level would be between E_F and −2 eV, probably closer to −2 eV. The relative intensity of the two $4f$ features changes across the temperature-dependent α-γ transition with unchanged overall intensity, suggesting a slight upward shift of the $4f$ level from the γ to the α phase, if the spectra are not sensitive to the change in the degree of localization of initial-state $4f$ in the phase transition. The XPS features just below E_F for Ce, which

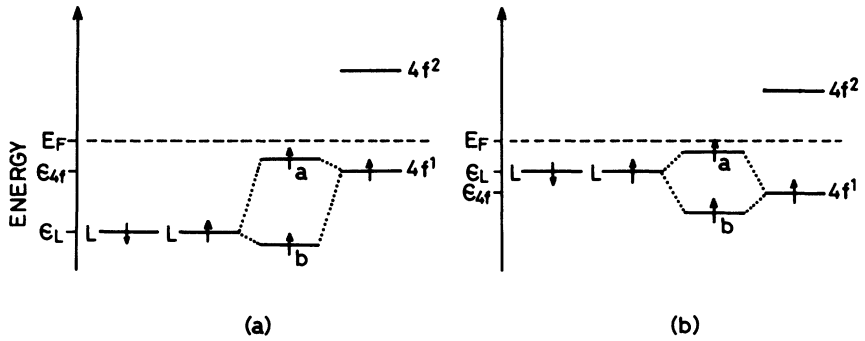

FIG. 3. "One-electron-like" energy levels for the initial ground state of Ce pnictides having integral valence of $4f^1$. The $4f^1$ level shifts so as to locate the antibonding level below E_F, thereby making the $4f$ occupation number unity. (a) Ligand level well below E_F as in CeP; (b) ligand level near E_F.

TABLE II. The energies of the "bare" Ce $3d_{5/2}$ level ϵ_{3d} and the core-hole–lowered $4f^2$ level ϵ'_{4f} for Ce pnictides obtained from observed binding energies of the main and satellite lines of Ce $3d_{5/2}$ using V in Table I. All energies in electron volts.

	Binding energies[a] E_B	ϵ_{3d}	$\epsilon'_{4f}-\epsilon_L$	$\epsilon'_{4f}-\epsilon_{4f}$
CeP	884.9,879.9	−884.6	−4.4	−5.4
CeAs	884.3,878.2	−884.0	−5.6	−5.6
CeSb[b]	884.5,878.2	−884.3	−5.9	−5.3

[a]Reference 9.

[b]ϵ'_{4f}, ϵ_L, and V for CeSb; mean values of those for CeP and CeBi were used.

are absent for La and Pr,[15] can thus be explained rather than by the presence of the $4f$ level just below E_F.

III. SATELLITES IN 3d CORE PHOTOEMISSION

Core XPS spectra of rare-earth compounds exhibit satellite structures arising from ligand-to-metal charge-transfer excitations.[16] In this section, it is shown that the two–final-state formulation can be applied to the satellite structures of core XPS spectra of rare-earth compounds. On creation of a core hole on a Ce atom, coexcitation from the ground-state $4f^1$ configuration to the $4f^2$-configuration–ligand-hole state takes place. These final states can be treated in a way parallel to that of Sec. II, and close relation with the $4f$ spectra will be shown. We will be concerned with the $3d$ core spectra in which the multiplet splittings do not complicate the spectra.

The initial state and the core-hole final state are given by

$$\Psi_I = |4f^n\rangle , \tag{10}$$

$$\Psi'_F = c_{F0}|4f^n\rangle' + \sum_l c_{Fl}\phi'_l , \tag{11}$$

$$\phi'_l = (1/\sqrt{2})\sum_\sigma \phi'_{l\sigma} = \sum_{i,j,\sigma} \Gamma^l_{ij}|4f^n L^{-1}_{i\sigma} 4f_{j\sigma}\rangle' , \tag{12}$$

where primes denote the presence of a $3d$ core hole. Equations (10)–(12) describe the $4f^n$ ion, $n=1$ corresponding to Ce. The second term in (11) has been represented using the basis set with n electrons in the $4f^n$ ground state and with the $(n+1)$th electron in the crystal-field levels. One can easily see that this is equivalent to the expression using the complete basis set $|L^{-1}_{i\sigma}(4f^{n+1})_j\rangle'$, as only states having the same symmetry as the first term $|4f^n\rangle'$ have to be retained in (11). Some terms in $|4f^n L^{-1}_{i\sigma} 4f_{j\sigma}\rangle'$ are identical to zero because of Pauli's principle except for $n=0$. The second term in (11) represents a correlated $4f^{n+1}$–ligand-hole complex. The line intensity is given in the sudden approximation by

$$I \simeq |\langle \Psi'_I|\Psi'_F\rangle\langle 3d|e\vec{r}|\epsilon l\rangle| \propto |c_{F0}|^2 , \tag{13}$$

which has the same form as the $4f$ emission intensity (4). The final-state Hamiltonian

$$H = \begin{bmatrix} -\epsilon_{3d} & V' \\ V' & -\epsilon_{3d}+\epsilon'_{4f}-\epsilon'_L \end{bmatrix} , \tag{14}$$

has the same form as (6) except that parameters for the core-hole state are used. ϵ'_{4f} is the $4f^{n+1}$ level

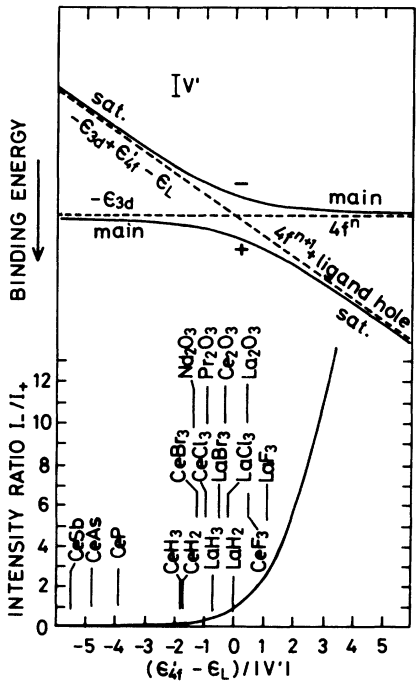

FIG. 4. Binding energies and intensity ratio of the main and satellite lines of the $3d$ core-level XPS spectra of rare-earth compounds as a function of $(\epsilon'_{4f}-\epsilon_L)/|V'|$. ϵ'_{4f} is the energy of the $4f^{n+1}$ level in the presence of the $3d$ core hole.

of the $3d$ core-ionized atom, and in the excited atom approximation[17] is the $4f^{n+1}$ level of the $Z+1$ atom. The ligand levels are relatively unaffected by the core hole, and we set $\epsilon'_L=\epsilon_L$. The binding energies of the two $3d$ features are obtained as

$$E_B=E_{\pm}=-\epsilon_{3d}+\{(\epsilon'_{4f}-\epsilon_L)\pm[(\epsilon'_{4f}-\epsilon_L)^2+4V'^2]^{1/2}\}/2\ , \quad (15)$$

and the intensity ratio as

$$I_-/I_+=|c_{0-}/c_{0+}|^2=\frac{(x'^2+4)^{1/2}+x'}{(x'^2+4)^{1/2}-x'}\ , \quad (16)$$

$$x'=(\epsilon'_{4f}-\epsilon_L)/|V'|\ , \quad (17)$$

as illustrated in Fig. 4.

The $3d$ spectra of the Ce pnictides[9] show weak satellites at binding energies 5–6 eV lower than the main lines. By assuming $V'\simeq V$, the bare Ce $3d_{5/2}$ binding energies and the energies of the $4f^{n+1}$ levels relative to the ligand level $\epsilon'_{4f}-\epsilon_L$ have been obtained for CeP, CeAs, and CeSb as in Table II and Fig. 4. As ϵ'_{4f} is lower than ϵ_{4f} by ~ 5 eV, $(\epsilon'_{4f}-\epsilon_L)/|V'|\sim -5$ resulting in the weak satellites. On going from CeP to CeAs to CeSb, the main-satellite separation increases and the satellite intensity becomes low. We note in Table II that $\epsilon'_{4f}-\epsilon_{4f}\simeq -5.5$ eV while a $Z+1$ estimate with complete screening[17] gives $\epsilon'_{4f}-\epsilon_{4f}\simeq\epsilon_{4f}$(Pr) $-\epsilon_{4f}$(Ce)$\simeq -2$ eV,[15] which is ~ 3.5 eV higher than that for the Ce pnictides. This fact suggests that the $3d$ hole in the Ce pnictides is not completely screened by $5d$ electrons as in metals. The $5d$ screening affects most the energy of the $3d$-hole state corresponding to the main ($4f^n$, "poorly screened") line by the process $3d^9 4f^n \rightarrow 3d^9 4f^n 5d$, while it is not important for the core-hole state corresponding to the satellite ($\underline{L}^{-1}4f^{n+1}$, "well-screened") line as the ligand hole is more extended. Thus the $5d$ screening lowers the energy of the $4f^n$ state, thus effectively raising $\epsilon'_{4f}-\epsilon_L$ in Eq. (14) or $\epsilon'_{4f}-\epsilon_{4f}$. It also reduces $|V'|$ through reduction of pure $4f^n$ component in $|4f^n\rangle'$. Therefore, the $5d$ screening decreases the binding energy of the main line and weakens the satellite line, resulting in deviations from the simple expressions presented here.

Relation between the $4f^{n+1}$ level relative to the ligand level $\epsilon'_{4f}-\epsilon_L$ and the relative intensity of the two $3d$ lines are seen for La and Ce halides.[18] For $LaBr_3$ and $LaCl_3$ the high–binding-energy line is more intense, while the reverse is observed for LaF_3. In these halides, though not cubic, the rare-earth ion is coordinated by six halogen atoms and the local structure is similar to the octahedral LX_6 cluster. The ligand-energy levels are estimated to be $\epsilon_{Br}\sim -5$ eV, $\epsilon_{Cl}\lesssim -5$ eV, and $\epsilon_F\sim -6$ eV. As incomplete $5d$ screening is expected for these halides, by assuming that $\epsilon'_{4f}-\epsilon_{4f}$ for incomplete $5d$ screening is lower than that for the completely screening by 3.5 eV as in the pnictides, the lowered $4f^1$ level in the La halides is estimated to be $\epsilon'_{4f}\simeq\epsilon_{4f}$(Ce) -3.5 eV$\simeq -5.5$ eV. This together with $|V'|\sim 1$ eV reproduces well the energy separations and the intensity ratios of the $3d$ features (Fig. 4). For Ce halides, ϵ'_{4f} is lower than that in the La halides and consequently the low–binding-energy lines are weaker.

The sesquioxides L_2O_3 (L=La, Ce, Pr and Nd) (Ref. 10) also provide a series showing a relationship between the $4f^{n+1}$-ligand energy separation and the relative intensity of the two $3d$ lines. For L_2O_3 we have to consider a LO_7 cluster having low symmetry. In this case $\epsilon_0\simeq -5.5$ eV and by assuming incomplete $5d$ screening we estimate ϵ'_{4f}(La) $\simeq\epsilon_{4f}$(Ce) -3.5 eV$\simeq -5.5$ eV, ϵ'_{4f}(Ce)$\simeq\epsilon_{4f}$(Pr) -3.5 eV$\simeq -7$ eV, etc. This accounts for the decrease in the low–binding-energy line for $La_2O_3\rightarrow Ce_2O_3\rightarrow Pr_2O_3\rightarrow Nd_2O_3$ and the relatively unchanged energy separation between the main and satellite peaks (Fig. 4). A decrease in $|V'|$ due to decreases in $4f$-ligand overlaps and to decreases in the number of nonzero terms in $|4f^n\underline{L}_{i\sigma}^{-1}4f_{j\sigma}\rangle$"s with increasing n is also responsible for this trend.

TABLE III. The energies of the "bare" La $3d_{5/2}$ level ϵ_{3d} and the core-hole–lowered $4f^1$ level ϵ'_{4f} relative to ϵ_L and the effective matrix element V' for La hydrides obtained from observed binding energies and intensity ratio of the main and satellite lines of La $3d_{5/2}$. All energies in electron volts.

	Binding energies[a] E_B	Intensity ratio[a] I_-/I_+	ϵ_{3d}	$\epsilon'_{4f}-\epsilon_L$	V'
LaH_2	837.1,835.1	~ 1	-836.1	0.0	1.0
LaH_3	838.7,835.0	~ 0.5	-837.5	-1.2	1.7

[a]Reference 11.

We should also like to discuss the $3d$ spectra of rare-earth metal hydrides LH_x ($2 \leq x \leq 3$), in which shifts of $4f$ levels and changes in the electronic structure with composition H-L have interesting effects. In the rare-earth hydrides electron charges are transferred from metal to hydrogen.[19–21] Energy shifts as large as 1.6 eV have been observed for LaH_x core levels for $2 \leq x \leq 3$, whereas a shift of only 0.2 eV is observed in CeH_x.[11] Therefore, a larger change in the unoccupied $4f^1$ level is expected for LaH_x, which would lead to pronounced changes in the $3d$ core spectra of LaH_x as compared to CeH_x. Actually no changes in the energy separation and the intensity ratio have been detected for Ce $3d$, while La $3d$ changes its features considerably between LaH_2 and LaH_3. "Bare" $3d_{5/2}$ energies and V' have been evaluated from the experimental energies and intensities as in Table III (see also Fig. 4). The rare-earth dihydrides and trihydrides have the CaF_2 and BF_3 structures, respectively. The rare-earth atom is coordinated by eight hydrogens at tetrahedral sites and by six additional hydrogens at octahedral sites in the trihydride (Fig. 5). $4f$ and ligand orbitals involved in the $L^{-1}4f^{n+1}$ state are a_{2u}-like and t_{1u}-like: For the tetrahedral hydrogen (a_{2u} and t_{1u}, respectively),

$$\phi'_{l\sigma}=(1/\sqrt{8})(s_1+s_3+s_6+s_8-s_2-s_4-s_5-s_7)xyz\ ,$$

$$\phi'_{m\sigma}=(1/\sqrt{3})\{(1/\sqrt{8})(s_1+s_2+s_3+s_4-s_5-s_6-s_7-s_8)[z^3-(\tfrac{3}{5})zr^2]$$
$$+(1/\sqrt{8})(s_1+s_2+s_5+s_6-s_3-s_4-s_7-s_8)[x^3-(\tfrac{3}{5})xr^2]$$
$$+(1/\sqrt{8})(s_2+s_3+s_6+s_7-s_1-s_4-s_5-s_8)[y^3-(\tfrac{3}{5})yr^2]\}\ ,$$

and, for the octahedral hydrogen (t_{1u}),

$$\phi'_{n\sigma}=(1/\sqrt{3})\{(1/\sqrt{2})(s_{13}-s_{14})[z^3-(\tfrac{3}{5})zr^2]+(1/\sqrt{2})(s_9-s_{10})[x^3-(\tfrac{3}{5})xr^2]$$
$$+(1/\sqrt{2})(s_{11}-s_{12})[y^3-(\tfrac{3}{5})yr^2]\}\ ,$$

where s_1 denotes the H $1s$ orbital on atom 1 (Fig. 5), etc. By neglecting the difference in the lattice parameters of CeH_x and LaH_x, V' for LaH_2 and LaH_3 can be evaluated from the energy-band calculations of CeH_2 and CeH_3,[20] in which linear combination of atomic orbitals parameters for Ce $4f$–H $1s$ interactions are given; one obtains $V'_l=1.89$ eV, $V'_m=1.49$, eV, and $V'_n=1.07$ eV. Thus for LaH_2, $V'=2.4$ eV and, for LaH_3, $V'=2.6$ eV, which is larger than the values in Table III, particularly for LaH_2. This discrepancy may be due to $5d$ screening effects on the main $3d$ lines. ϵ_L can be related to energy bands as $\epsilon^l_L(a_{2u}) \simeq \epsilon(\Gamma'_2)$, $\epsilon^m_L(t_{1u}) \simeq \epsilon(X'_4)$, and $\epsilon^n_L(t_{1u}) \simeq \epsilon(\Delta_1(\frac{1}{2}00))$. These energy levels correspond roughly to the midpoint between the DOS peak of the hydrogen-induced valence band and E_F (Refs. 19–21): $\epsilon_L \simeq -3$ eV.

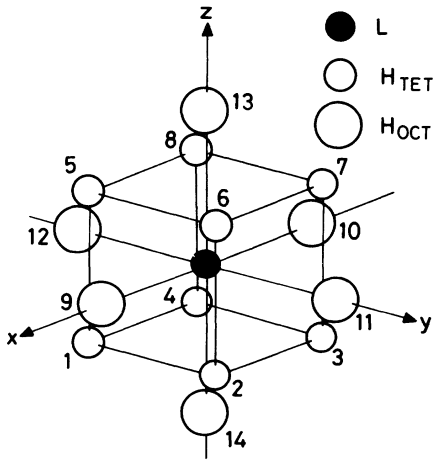

FIG. 5. Structure of the LH_8 or LH_{14} cluster representing local environment of the rare-earth ion in fcc rare-earth hydrides. For the dihydride there are only tetrahedral hydrogens, and for the trihydride both tetrahedral and octahedral hydrogens are present.

It is interesting to note that for LaH_x the $Z+1$ approximation with complete screening gives a better estimate of ϵ'_{4f} as compared to the case of the rare-earth pnictides, hydrides, halides, and oxides: In the $Z+1$ approximation with complete screening for LaH_x, $\epsilon'_{4f}-\epsilon_L \simeq \epsilon_{4f}(\mathrm{Ce})-\epsilon_L \simeq 1$ eV, where $\epsilon_{4f}(\mathrm{Ce})$ is the $4f$ energy from the valence-band XPS of CeH_x.[11] That is, $\epsilon'_{4f}-\epsilon_L$ in Table III is lower than the $Z+1$ estimate with complete screening by ~ 2 eV for LaH_3 and by only ~ 1 eV for metallic LaH_2. This fact would also indicate that in metallic LaH_2 the screening of the $3d$ hole by $5d$ electrons is much more effective than other rare-earth compounds because of the high $5d$-like DOS at E_F even in semiconducting LaH_3 because of the high $5d$ DOS just above the narrow band gap.[19–21] The

difference in $\epsilon'_{4f}-\epsilon_L$ between LaH_2 and LaH_3 is compared with the core-level shifts as in Table III. Different $5d$ screening could also contribute to the difference in $\epsilon'_{4f}-\epsilon_L$, although the $5d$ screening and the core-level shift cannot be separated experimentally.

In Fig. 4 behavior of the $3d$ XPS of the rare-earth compounds discussed in this section are plotted. As one moves in the figure from $\epsilon'_{4f}-\epsilon_L=0$ to the left, separation between the main line and the satellite line at lower binding energies increases and the relative intensity of the satellite decreases. These satellites originate from the $L\rightarrow 4f$ shakedown process. In the region near $\epsilon'_{4f}-\epsilon_L\simeq 0$ the separation between the two lines is rather constant $\sim 2|V'|$, while the relative intensity varies most sensitively with $\epsilon'_{4f}-\epsilon_L$. As one moves to $\epsilon'_{4f}-\epsilon_L>0$, the satellite appears at higher binding energies as in La_2O_3 and LaF_3, and the satellites may be thought of as arising from the $L\rightarrow 4f$ *shakeup* process. That is, the well-screened peak appears at higher binding energies than the poorly screened peak, which is a different assignment for La_2O_3 than that in Ref. 10. Moreover, it can be said that for $\epsilon'_{4f}-\epsilon_L\sim 0$ it is not meaningful to tell which is the main (poorly screened) line and to regard this line as representing well chemical shifts.

IV. FINAL STATE OF BREMSSTRAHLUNG-ISOCHROMAT SPECTROSCOPY

We would like to suggest the possibility of hybridization of two final states of BIS, which could give additional spectral features. Because of the rather extended nature of the empty levels in the metallic systems studied by BIS, the two–final-state approach using cluster models as in Secs. II and III is only schematic in this case.

The BIS spectra for γ-Ce, $CeSn_3$, and $CePd_3$, but not for $CeAl_3$ and La,[12] have shown high intensities just above E_F that cannot be explained by the empty DOS of valence states. This extra BIS feature has been attributed to the empty $4f^1$ level, suggesting an occupied $4f^1$ level just below E_F. However, this is in conflict with another photoemission experiment that locates the $4f^1$ level of γ-Ce about 2 eV below E_F.[14,22] Moreover, the absence of the empty $4f^1$ level in $CeAl_3$ and, consequently, the occupied $4f^1$ level well below E_F may be inconsistent with the $4f^2$ BIS energy which is higher than γ-Ce and $CeSn_3$ and as high as mixed-valent $CePd_3$ for which the occupied $4f^1$ level should be near E_F.

We tentatively attribute this extra BIS intensity to final-state effects resulting from hybridization between two configurations, a localized $4f^2$ state and a delocalized state with the incident electron in empty valence levels. In the BIS of Ce and $CeSn_3$, the latter state gets BIS intensity through mixing with the $4f^2$ configuration which has large BIS cross sections. Strong hybridization can stem from energetic proximity and large overlap between the two final-state configurations. In this respect, the empty $4f^1$ level of La (Refs. 15 and 23) is too high (~ 5 eV above E_F) to cause the mixing, while in Ce the $4f^2$ level is 3–4 eV above E_F, which is near the empty valence region.

As in Secs. II and III we write the initial and the final states as follows, neglecting multiplet splittings and other final-state structures:

$$\Psi_I=|4f^n\rangle\ , \tag{18}$$

$$\Psi_F=c_{F0}|4f^{n+1}\rangle+c_{Fl}|v4f^n\rangle\ , \tag{19}$$

where v denotes an electron in an empty valence level. The energies of the final states are

$$E_f=E_{\pm}=[(\tilde{\epsilon}_{4f}+\epsilon_v)\pm[(\tilde{\epsilon}_{4f}-\epsilon_v)^2+4\tilde{V}^2]^{1/2}\}/2\ , \tag{20}$$

where $\tilde{\epsilon}_{4f}$ and ϵ_v are the energies of the $4f^{n+1}$ level and the empty valence level, respectively, and $\tilde{V}=\langle 4f^{n+1}|H|v4f^n\rangle$. The Ce atom is surrounded

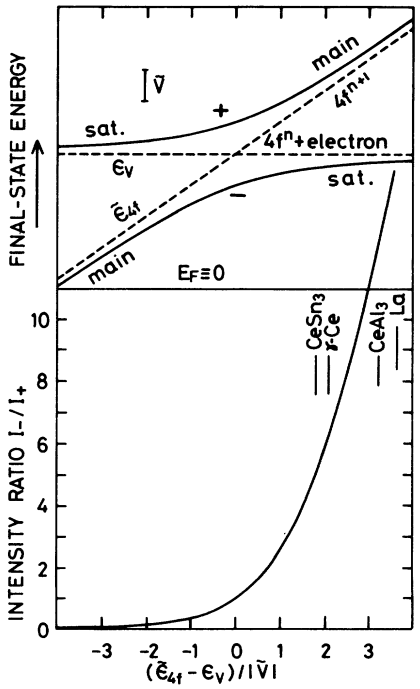

FIG. 6. Final-state energies and intensity ratio of two bremsstrahlung-isochromat spectral features as a function of $(\tilde{\epsilon}_{4f}-\epsilon_v)/|\tilde{V}|$. $\tilde{\epsilon}_{4f}$ and ϵ_v are the energies of the empty $4f^{n+1}$ and valence levels, respectively.

by twelve Ce atoms in γ-Ce and twelve X atoms in CeX_3-type alloys, and the empty valence levels are Ce $5d$-like for γ-Ce (Ref. 24) and X p-like for CeX_3.[25] For the primary electron energy used in the BIS experiment[12] cross section for $\epsilon l \rightarrow 4f$ dominates, giving the BIS intensity of

$$I \simeq |c_{F0}\langle 4f | e\vec{r} | \epsilon l\rangle|^2 \propto |c_{F0}|^2 . \quad (21)$$

Equations (20) and (21) vary with $(\tilde{\epsilon}_{4f}-\epsilon_v)/|\tilde{V}|$ as shown in Fig. 6. Although $\tilde{V}$ and ϵ_v for the unoccupied valence states are not well known, it is evident from the $4f^2$ energy in BIS that $\tilde{\epsilon}_{4f}-\epsilon_v$ is larger for $CeAl_3$ than for γ-Ce and $CeSn_3$. The trend in the relation between $\tilde{\epsilon}_{4f}-\epsilon_v$ and the satellite intensity is well explained in Fig. 6, where $(\tilde{\epsilon}_{4f}-\epsilon_v)/|\tilde{V}|$ roughly deduced from experimental intensities is indicated.

In the case of mixed-valent $CePd_3$, the $4f^1$ and $4f^0$ configurations are degenerate in the initial state:

$$\Psi_I = a\,|4f^1\rangle + b\,|4f^0\rangle . \quad (22)$$

The final state is

$$\Psi_F = c_{F0}\,|4f^2\rangle + c_{Fl}(a\,|v4f^1\rangle + b\,|v4f^0\rangle) + c_{Fm}\,|4f^1\rangle . \quad (23)$$

Here the first term and the last term represent, respectively, the localized $4f^2$ and $4f^1$ configurations and the second term represents the state with the incident electron in the empty valence states without perturbing the initial-state mixed-valent Ce ions. The $4f^1$ final state is just above E_F as expected for the mixed-valent system and the valence-electron final state is expected to overlap the $4f^1$ state or to be between the $4f^1$ and $4f^2$ final states. Owing to hybridization between the three final states, transition to the valence-electron state gets BIS intensity through admixture with $4f^1 \rightarrow 4f^2$ and principally with $4f^0 \rightarrow 4f^1$ components. We identify the peak about 2 eV above E_F with the valence-electron state rather than with a surface feature of $4f^2$, as the intensity and the energy shift with respect to the bulk $4f^2$ can hardly be explained by the surface effect.

Thus the final-state effects account for the BIS of Ce and its alloys in a more natural way than the previous assignment using empty $4f^1$ states. Here the second term in (19), $|v4f^n\rangle$, needs more specification. $|4f^2\rangle$ has been identified as the localized $4f^2$ configuration screened by $5d$ holes. v in $|v4f^n\rangle$ is not necessarily a bandlike electron but may be a weakly localized electron on neighbor atoms of the $4f$ ion. Then the BIS satellite can be regarded as arising from a $4f$-hole—valence-electron pair excited simultaneously with the $4f^1 \rightarrow 4f^2$ transition. This is the electron-hole reversal of the $4f$ photoemission discussed in Sec. II. For unambiguous identification of the BIS spectra, further studies taking into account the electronic structure of γ-Ce and the CeX_3 alloys are necessary.

ACKNOWLEDGMENT

The author is grateful to L. Schlapbach for providing copies of his work prior to publication.

[1] C. Varma, Rev. Mod. Phys. 48, 219 (1976); J. H. Jefferson and K. W. H. Stevens, J. Phys. C 11, 3919 (1978); *Valence Instabilities and Related Narrow-Band Phenomena*, edited by R. D. Park (Plenum, New York, 1977).

[2] *Photoemission in Solids I*, Vol. 26 of *Topics in Applied Physics*, edited by M. Cardona and L. Ley (Springer, Berlin, 1979).

[3] S. Hüfner and G. K. Wertheim, Phys. Lett. 24A, 299 (1975); C. Guillot, Y. Ballu, J. Paigué, J. Lecante, K. P. Jain, P. Thiry, R. Pinchaux, Y. Pétroff, and L. M. Falikov, Phys. Rev. Lett. 39, 1632 (1977).

[4] M. Iwan, F. J. Himpsel, and D. E. Eastman, Phys. Rev. Lett. 43, 1829 (1979).

[5] M. Iwan, E. E. Koh, T. C. Chang, and F. J. Himpsel, Phys. Lett. 76A, 177 (1980).

[6] L. C. Davis, Phys. Rev. B 25, 2912 (1982).

[7] A. Franciosi, J. H. Weaver, N. Mårtensson, and M. Croft, Phys. Rev. B 24, 3651 (1981).

[8] J. Brunner, M. Erbudak, and F. Hulliger, Solid State Commun. 38, 841 (1981).

[9] Y. Baer, R. Hauger, Ch. Zürcher, M. Campagna, and G. K. Wertheim, Phys. Rev. B 18, 4433 (1978).

[10] J. C. Fuggle, M. Campagna, Z. Zolnierek, R. Lässer, and A. Plateau, Phys. Rev. Lett. 45, 1597 (1980); C. K. Jørgensen and H. Berthou, Chem. Phys. Lett. 13, 186 (1972).

[11] L. Schlapbach and H. R. Scherrer, Solid State Commun. 41, 893 (1982); L. Schlapbach and J. Osterwalder, *ibid.* 42, 271 (1982); L. Schlapbach, J. Osterwalder, and H. C. Siegmann, J. Less-Common Met. 88, 291 (1982); A. Fujimori and N. Tsuda; Phys. Status Solidi B (in press).

[12] Y. Baer, H. R. Ott, J. C. Fuggle, and L. E. DeLong, Phys. Rev. B 24, 5384 (1981).

[13] A. Hasegawa and A. Yanase, J. Phys. Soc. Jpn. 42, 492 (1977).

[14] N. Mårtensson, B. Rheil, and R. D. Parks, Solid State Commun. 41, 573 (1982).

[15] J. K. Lang, Y. Baer, and P. A. Cox, J. Phys. F 11, 121 (1981).

[16] M. Campagna, G. K. Wertheim, and Y. Baer, in *Photo-*

emission in Solids II, Vol. 27 of *Topics in Applied Physics,* edited by L. Ley and M. Cardona (Springer, Berlin, 1979), p. 217.

[17]B. Johansson, Phys. Rev. B 20, 1315 (1979); B. Johansson and N. Mårtensson, *ibid.* 24, 4484 (1981).

[18]A. J. Signorelli and R. G. Hayes, Phys. Rev. B 8, 81 (1973); S. Suzuki, T. Ishii, and T. Sagawa, J. Phys. Soc. Jpn. 37, 1334 (1974).

[19]A. C. Switendick, J. Less-Common Met. 74, 199 (1980).

[20]A. Fujimori, F. Minami, and N. Tsuda, Phys. Rev. B 22, 3573 (1980); A. Fujimori and N. Tsuda, Solid State Commun. 41, 491 (1982).

[21]M. Gupta and J. P. Burger, Phys. Rev. B 22, 6074 (1980).

[22]J. W. Allen, S. J. Oh, I. Lindau, J. M. Lawrence, L. I. Johansson, and S. B. Hagström, Phys. Rev. Lett. 46, 1100 (1981).

[23]J. K. Lang, Y. Baer, and P. A. Cox, Phys. Rev. Lett. 42, 74 (1979).

[24]D. Glötzel and L. Fritsche, Phys. Status Solidi B 79, 85 (1977).

[25]D. M. Gray and L. V. Meisel, Phys. Rev. B 5, 1299 (1972); D. D. Koelling, Solid State Commun. 43, 247 (1982).